Journal of Organometallic Chemistry 760 (2014) 248–259

Contents lists available at ScienceDirect

Journal of Organometallic Chemistry

journal homepage: www.elsevier.com/locate/jorganchem

Structural and optical properties of new cyclometalated Ru(II) derived compounds

Sidonie Finck [a], Jean-Thomas Issenhuth [b], Stéphane Despax [b,c], Claude Sirlin [b], Michel Pfeffer [b], Corentin Poidevin [a], Christophe Gourlaouen [a], Alex Boeglin [c], Chantal Daniel [a,*]

[a] Laboratoire de Chimie Quantique, Institut de Chimie CNRS – Université de Strasbourg, 1 Rue Blaise Pascal, 67 070 Strasbourg-Cedex, France
[b] Laboratoire de Synthèses Métallo-Induites, Institut de Chimie CNRS – Université de Strasbourg, 1 Rue Blaise Pascal, 67 070 Strasbourg-Cedex, France
[c] Département d'Optique Ultra-Rapide et de Nano-Photonique, IPCMS, UMR 7504, CNRS – Université de Strasbourg, 23 Rue du Loess, BP 84087, 67 034 Strasbourg Cedex 2, France

ARTICLE INFO

Article history:
Received 25 June 2013
Received in revised form
13 August 2013
Accepted 16 August 2013

Keywords:
Cyclometalated ruthenium complexes
Absorption spectroscopy
Structural properties
Excited states
Time-dependent density functional calculations

ABSTRACT

The electronic spectra of 4 cyclometalated ruthenium compounds built up from cycloruthenated 2-phenylpyridine with monodentate and bidentate ligands, namely **1** $[Ru(MeCN)_2(phen)(PhPy)]^{1+}$ (**RDC11**), **2** $[Ru(phen)_2(PhPy)]^{1+}$ (**RDC34**), **3** $[Ru(MeCN)_2(PhPy)(dppz)]^{1+}$ (**RDC11Z**), **4** $[Ru(bpy)(PhPy)(dppz)]^{1+}$ (**RDCbpZ**), the last two being newly synthesized, have been recorded and calculated together with that of **5** $[Ru(bpy)_2(dppz)]^{2+}$ (**RDNbpZ**). Recently synthesized variants of **RDC34** where the phenylpyridine ligand is substituted with an electro-attractor or an electro-donor group, **6** $[Ru(phen)_2(NO_2PhPy)]^{1+}$ **RDC40** and **7** $[Ru(phen)_2(NH_2PhPy)]^{1+}$ **RDC41** respectively, and the dicationic reference complex $[Ru(phen)_2(bpy)]^{2+}$ (**RDN34**) have been investigated as well for comparison. The global structures of **RDC34** and **RDN34** are very similar despite of the substitution of one N atom by one C atom. As expected a shortening of the Ru–C bond as compared to the Ru–N bond is observed. The calculated structures of the investigated complexes point to a rather rigid structure whatever their environment. The introduction of a strong Ru–C bond has a minor effect on the coordination sphere around the metal atom keeping the other Ru–N bonds and bond angles similar, the only noticeable alteration being an increase of the Ru–N bond trans to the Ru–C bond. The experimental spectra are characterized by an intense band in the UV domain centered at 270 nm and corresponding to a strong intra-ligand (IL) absorption. Low-lying MLCT states contribute to a weak shoulder around 370 nm and to a large band between 550 nm and 400 nm. The tail of this band, towards 650 nm, is a characteristic of the cyclometalated complexes. This series of molecules, as other polypyridyl complexes, are characterized by a high density of excited states in the vis/UV energy domain, a large mixing between MLCT/IL and LLCT states in the upper part of the spectrum, and a significant sensitivity to the environment of the IL state localized on the dppz ligands.

1. Introduction

Cyclometalated complexes of ruthenium(II) have often been considered to be interesting organometallic molecules because they display properties that may find useful applications in several domains of chemistry, physics or biology [1]. For example, they have been found to be (*i*) important intermediates in the ortho functionalization of aromatics via CH activation [2], (*ii*) good catalyst precursors for several catalytic processes, especially the asymmetric reduction of ketone and imines [3], (*iii*) efficient dyes in dye-sensitized solar cells [4], and (*iv*) powerful electronic relays in enzyme mediated redox processes thanks to their electronic properties [5]. Moreover, these compounds have also been shown to display *in vitro* and *in vivo* cytotoxic properties against several tumor cell lines at levels significant enough to consider them as potential anticancer drugs candidates [6].

In the early stages of our investigations into their mode of action against several cancer cell lines, it appeared that interactions with DNA could be invoked to partially explain the apoptotic behavior of cells treated with solutions of these compounds (at the μMol

* Corresponding author.
E-mail address: c.daniel@unistra.fr (C. Daniel).

0022-328X/$ – see front matter © 2013 Published by Elsevier B.V.
http://dx.doi.org/10.1016/j.jorganchem.2013.08.032

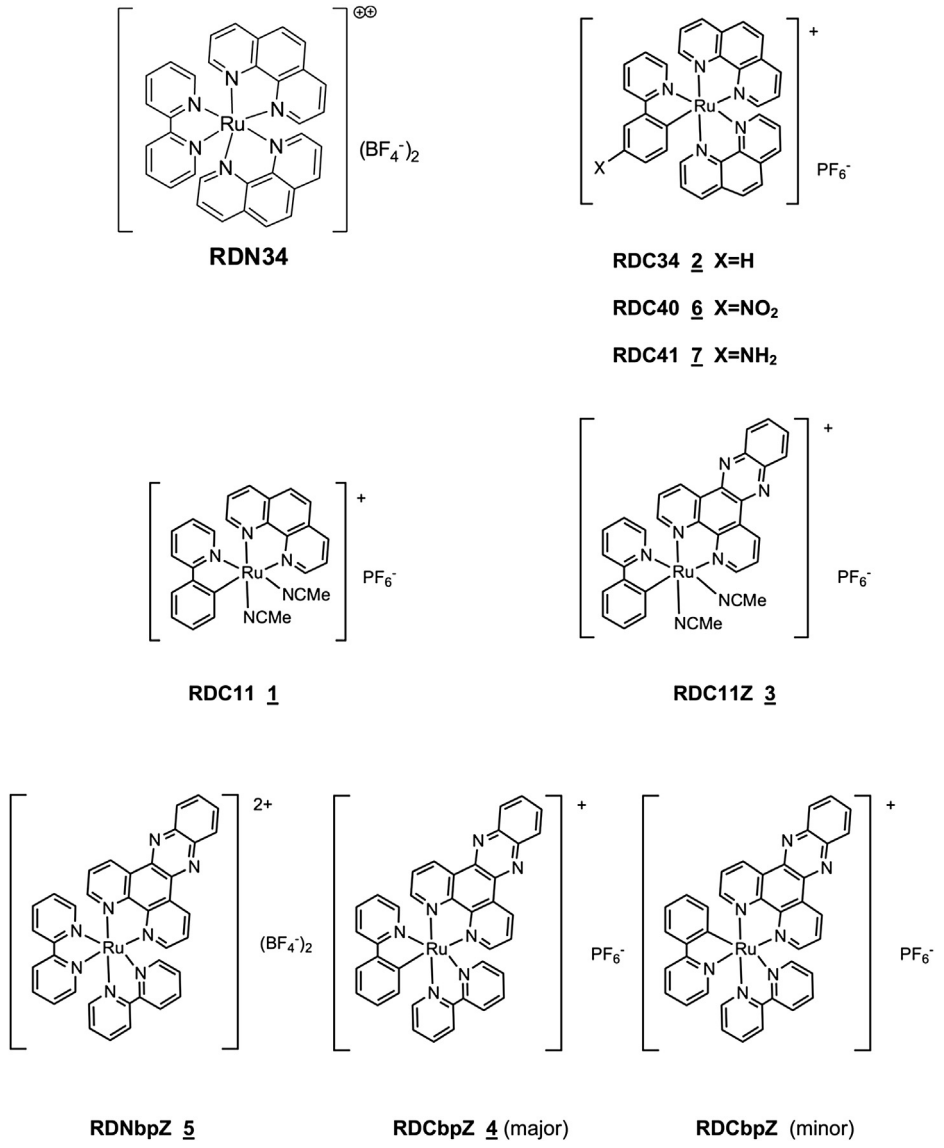

Chart 1.

(micromolar) level). However, we had also found that direct coordination of the DNA via any of its pair bases had to be ruled out: as we used ruthenium compounds whose coordination sphere was saturated, no free coordination sites being available on the ruthenium center.

In particular, the ruthenium complexes $[Ru(MeCN)_2(phen)(PhPy)]^{1+}$ (**1**, referred to as **RDC11** in the text) and $[Ru(phen)_2(PhPy)]^{1+}$ (**2**, referred to as **RDC34**) (MeCN = acetonitrile; Phpy = phenyl-pyridine; phen = 1,10-phenanthroline) have demonstrated cytotoxic properties [6b]. Furthermore these complexes were shown to interact with DNA by intercalation of the phenanthroline ligand [7]. The addition of a second phenanthroline in **RDC34** significantly increased the cytotoxicity. Also the modification of its Phpy ligand by addition of NO_2 or NH_2 in the newly synthesized variants of **RDC34** $[Ru(phen)_2(NO_2PhPy)]^{1+}$ **6** (**RDC40**) and $[Ru(phen)_2(NH_2PhPy)]^{1+}$ **7** (**RDC41**) [6d], improves significantly the water solubility and eventually the cytotoxicity [6e].

Another aspect concerns the optical properties of the ruthenium derived compounds (RDC), more particularly the quenching of luminescence by concurrent electron transfer. This is the molecular light switch effect potentially controlled by the environment as discovered by Barton et al. for $[Ru(bpy)_2(dppz)]^{2+}$ (bpy = 2,2′-bipyridine; dppz = dipyrido(3,2-a:2′,3′-c)phenazine) [8], complex **5** (**RDNbpZ**) in the present work. Despite the number of recent experimental studies by means of various spectroscopic techniques, the response of these metallo-intercalators to visible light is far from being understood and rationalized. Theoretical works dedicated to the electronic excited-state properties of this class of ruthenium complexes taking into account the environment (solvent, synthetic polynucleotide or DNA) are still scarce [9]. In a recent article [10], we have proposed a detailed theoretical study of the absorption spectroscopy of the two isolated complexes $[Ru(phen)_2dppz]^{2+}$ and $[Ru(tap)_2dppz]^{2+}$ (tap = 1,4,5,8-tetraazaphenanthrene) which exemplify the two extreme behaviors upon visible irradiation when intercalated in DNA, namely an enhanced luminescence for the phen complex vs. a photo-induced electron transfer for the tap substituted molecule [11].

The purpose of this joined experimental/theoretical study is to investigate in details the structure and electronic spectra of a series of newly synthesized RDC possessing a dipyridophenazine (dppz)

ligand, a well known intercalator of DNA [12]. The optical properties of previously synthesized complexes which have proved valuable for their cytotoxic properties are reported as well for comparison. The complexes are represented in Chart 1. The ordinal numbers are given for the sake of clarity of the different figures. In the Results and discussion section the complexes will be referred according to the RDC nomenclature of the published library [6d].

2. Experimental section

The experimental details for the synthesis and the characterization of the synthesized complexes are the same as those described in a previous paper [6d]. The various starting materials mentioned throughout were obtained according to published procedures.

2.1. Synthesis of [Ru(dppz)(NCMe)$_2$(2-PhPy)]$^+PF_6^-$ (RDC11Z, **3**)

To a solution of [Ru(2-Ph-2′-Py)(MeCN)$_4$]PF$_6$ [13] in CH_2Cl_2 was added dipyrido[3,2-*a*:2′,3′-*c*]phenazine (1 eq.) and the solution was stirred and refluxed for 24 h. During this period, the color of the solution changed from yellow to dark red. This solution was concentrated in vacuo and the resulting solid was dissolved in CH_2Cl_2, precipitated by the addition of pentane and washed with pentane. The resulting dark red solid was collected and filtered over Al_2O_3 using CH_3CN/CH_2Cl_2 (10%) as eluent. A dark red fraction was collected and was concentrated (and dried) in vacuum. Yield: 40%.

HRMS (ES, *m*/*z*): calculated for $C_{31}H_{24}N_7Ru$: 620.114, found 620.115; calculated for (M − CH_3CN) 579.087, found 579.087.

^{1}H NMR (500 MHz, CD_3CN, 300 K): δ = 9.79 (dd, 1H, ^3J = 5.3, ^4J = 1.5 Hz), 9.54 (dd, 1H, ^3J = 8, ^4J = 1.5 Hz), 8.95 (dd, 1H, ^3J = 7.9, ^4J = 1.1 Hz), 8.32 (dd, 1H, ^3J = 7.3, ^4J = 1 Hz), 8.27 (m, 2H), 8.21 (dd, 1H, ^3J = 5.5, ^4J = 1.1 Hz), 8.18 (dd, 1H, ^3J = 8, ^4J = 1.8 Hz), 8 (m, 2H), 7.92 (m, 2H), 7.59 (dd, 1H, ^3J = 6, ^4J = 1 Hz), 7.53 (ddd, 1H, ^3J = 7.4, ^3J = 9.7, ^4J = 1.3 Hz), 7.32 (m, 1H), 7.32 (m, 1H), 7.14 (ddd, 1H, ^3J = 8, ^4J = 1.1 Hz), 6.7 (ddd, 1H, ^3J = 5.8, ^3J = 7.4, ^4J = 1.3 Hz), 2.32 (s, 3H) and 2.12 (s, 3H).

^{13}C NMR (125 MHz, CD_3CN, 300 K): δ = 192.18, 169.56, 157.65, 153.68, 153.05, 152.36, 150.12, 146.77, 143.40, 143.33, 141.05, 140.85, 139.07, 136.79, 133.21, 132.95, 131.50, 130.44, 130.38, 129.47, 128.16, 126.22, 126.04, 124.94, 123.02, 122.12, 121.78, 119.04, 118.29, 4.52, 4.19.

2.2. Synthesis of Ru(2,2′-bipy)(dppz)Cl$_2$

[Ru(2,2′-bipy)(NCMe)$_3$Cl]$^+Cl^-$ + Ru(2,2′-bipy)(NCMe)$_2$Cl$_2$ were synthesized according to a published procedure [9]. To a solution of the mixture of these 2 compounds (100 mg) in 25 mL of acetone was added dppz (69 mg, 1 eq.) and the solution was stirred and refluxed for 15 h. During this period the solution changed color from red to dark purple. The resulting solution was concentrated in vacuum. Then the resulting dark purple solid was dissolved in CH_2Cl_2, precipitated by the addition of pentane and washed with pentane and acetonitrile.

2.3. Synthesis [Ru(2,2′-bipy)(dppz)(2-PhPy)]$^+PF_6^-$ (RDCbpZ, **4**)

Ru(bpy)(dppz)Cl$_2$ (187 mg, 0.3 mmol), phenylpyridine (43 μL, 0.3 mmol), tetramethylammonium hydroxide (108.8 mg, 0.6 mmol) and $AgPF_6$ (227.55 mg, 0.9 mmol) were refluxed in dichloromethane (20 mL) for 24 h at 45 °C. The reaction mixture was evaporated. The complex was purified by column chromatography over Al_2O_3, 10% CH_3CN/CH_2Cl_2 as eluent and concentrated in vacuum. A deep purple solid (mixture of two isomers) was obtained. Yield: 20%.

2.4. Synthesis of [Ru(2,2′-bipy)(dppz)(2-PhPy)]$^+CF_3SO_3^-$

A similar procedure in which $AgPF_6$ was replaced by the same equivalent of AgOTf was used to obtain the derivative that afforded mono crystals amenable for the X-ray diffraction study. The analytical data of this compound having an OTf (OTf = CF_3SO_3) as counteranion, were the same as those of the PF_6 containing compound.

HRMS (ES, *m*/*z*): calculated for $C_{39}H_{26}N_7Ru$: 694.129, found 694.090.

^{1}H NMR (500 MHz, CD_3CN, 300 K): δ = 9.43 (dd, 1H, ^3J = 8.1 Hz, ^4J = 1.4 Hz), 9.23 (dd, 1H, ^3J = 8.1 Hz, ^4J = 1.4 Hz), 9.18 (dd, 0.5H, ^3J = 8.1 Hz, ^4J = 1.4 Hz), 8.98 (dd, 0.5H, ^3J = 8.1 Hz, ^4J = 1.4 Hz), 8.47 (d, 0.5H, ^3J = 8.3 Hz), 8.43 (d, 0.5H, ^3J = 8.3 Hz), 8.40 (dd, 1.1H, ^3J = 5.4 Hz, ^4J = 1.3 Hz), 8.36–8.29 (m, 5.7H), 8.25–8.19 (m, 1.6H), 8.16 (ddd, 1.1H, ^3J = 7.6 Hz, ^3J = 5.4 Hz, ^4J = 1.1 Hz), 8.09–8.00 (m, 5.2H), 7.96–7.74 (m, 8.6H), 7.71–7.61 (m, 4.6H), 7.58 (dd, 1.2H, ^3J = 5.2 Hz, ^3J = 8.2 Hz), 7.44 (dd, 0.6H, ^3J = 5.2 Hz, ^3J = 8.2 Hz), 7.28 (m, 2.1H), 7.1 (ddd, 1.2H, ^3J = 7.9 Hz, ^3J = 6 Hz, ^4J = 1.2 Hz), 7.0 (ddd, 0.5H, ^3J = 7.3 Hz, ^3J = 5.8 Hz, ^4J = 1.2 Hz), 6.94–6.85 (m, 4.1H), 6.82 (ddd, 1.1H, ^3J = 7.3 Hz, ^3J = 5.8 Hz, ^4J = 1.2 Hz), 6.76 (td, 0.5H, ^3J = 7.4 Hz, ^4J = 1.2 Hz), 6.51 ppm (m, 1.6H).

^{13}C NMR (125 MHz, CD_3CN, 300 K): δ = 191.90, 167.39, 167.26, 157.80, 156.90, 156.73, 155.85, 155.10, 154.32,151.95, 151.72, 151.41, 151.02, 150.74, 150.64, 150.57, 150.37, 149.52, 148.84, 145.69, 142.43, 142.23, 140.26, 136.52,135.84, 135.64, 135.40, 135.24, 134.04, 133.90, 132.01, 131.85, 130.43, 130.24, 129.82, 129.69, 129.46, 129.37, 129.29, 128.82, 128.52, 127.03, 126.93, 126.45, 126.30, 126.13, 124.17, 123.53, 123.09, 122.97, 122.41, 122.25, 121.08, 118.94, 118.86 ppm.

Table 1
Crystallographic data for compounds **4** and **5**.

Complex	[Ru(bpy)$_2$(dppz)]$^{2+}$(BF$_4^-$)$_2$ RDNbpz **5**	[Ru(2,2′bipy)(PhPy)(dppz)]$^+CF_3SO_3^-$ RDCbpz **4**
Formula	2(C_{38} $H_{26}N_8Ru$), CH_2Cl_2, 4(BF_4)	2($C_{39}H_{26}N_7Ru$), 0.5($C_2F_6O_6S_2$), CF_3O_3S
Formula Weight	1823.64	1685.62
Crystal system	Triclinic	Monoclinic
Space group	'*P*-1'	'*P*21/c'
a (Å)	13.389(2)	20.6179(8)
b (Å)	17.165(3)	16.7207(6)
c (Å)	21.207(4)	24.4317(7)
Alpha (°)	98.968(4)	90.00
Beta (°)	105.204(4)	124.580(2)
Gamma (°)	107.591(4)	90.00
V (A^3)	4334.5(12)	6934.7(4)
Z	2	4
Density (g cm^{-3})	1.397	1.615
μ (mm^{-1})	0.495	0.581
F (000)	1828	3408
Data collection		
Temperature (K)	173(2)	173(2)
θ (min–max)	2.50–27.38	1.20–27.52
Dataset [*h*, *k*, *l*]	−17/17, −22/22, −26/27	−26/26, −21/20, −31/23
Tot., Uniq. Data, *R*(int)	51,038, 0.0447, 0.0693	48,544, 0.0887, 0.1111
Observed data (>2σ(*I*))	12,340	8313
Refinement		
N reflections, *N* parameters	19,831, 1048	15,928, 949
*R*2, *R*1, *wR*2, *wR*1, Goof	0.1510, 0.1067, 0.3243, 0.2997, 1.095	0.1764, 0.0945, 0.3087, 0.2516, 1.051
Max. and Av.	0.000, 0.000	0.000, 0.000

2.5. Crystal structure determination of **4** and **5**

The crystals were placed in oil, and a single crystal was selected, mounted on a glass fibre and placed in a low-temperature N_2

stream. X-Ray diffraction data collection was carried out on a Bruker APEX II DUO Kappa-CCD diffractometer equipped with an Oxford Cryosystem liquid N_2 device, using Mo-Kα radiation (λ = 0.71073 Å). The crystal-detector distance was 38 mm. The cell parameters were determined (APEX2 software) [14a] from reflections taken from tree sets of 12 frames, each at 10 s exposure. The structures were solved by direct methods using the program SHELXS-97 [14b]. The refinement and all further calculations were carried out using SHELXL-97 [14c]. The H-atoms were included in calculated positions and treated as riding atoms using SHELXL default parameters. The non-H atoms were refined anisotropically, using weighted full-matrix least-squares on F^2. A semi-empirical absorption correction was applied using SADABS in APEX2 [14a]; transmission factors: *T*min/*T*max = 0.8448/0.9715 for compound **4** and *T*min/*T*max = 0.9076/0.9430 for compound **5**. For compound **4**, one triflate anion is disordered over two positions. For compound **5**, the SQUEEZE instruction in PLATON [14d] was applied. The residual electron density was assigned to one molecule of dichloromethane.

2.6. Computational details

The geometrical structures of **1** $[Ru(MeCN)_2(phen)(PhPy)]^{1+}$ (**RDC11**), **2** $[Ru(phen)_2(PhPy)]^{1+}$ (**RDC34**), **3** $[Ru(MeCN)_2(PhPy)(dppz)]^{1+}$ (**RDC11Z**), **4** $[Ru(bpy)(PhPy)(dppz)]^{1+}$ (**RDCbpZ**), **5** $[Ru(bpy)_2(dppz)]^{2+}$ (**RDNbpZ**), **6** $[Ru(phen)_2(NO_2PhPy)]^{1+}$ (**RDC40**), **7** $[Ru(phen)_2(NH_2PhPy)]^{1+}$ (**RDC41**), (Chart 1), and $[Ru(phen)_2(bpy)]^{2+}$ (**RDN34**), have been optimized in vacuum, water, and acetonitrile, by means of density functional theory (DFT) with the B3LYP functional [15,16]. The optimized bond lengths with the PBE functional [17] lead to very small fluctuations (less than 2%) of the Ru–N and Ru–C distances in RDC34 (see Table 2). Relativistic pseudopotentials of Dresden/Stuttgart and associated valence basis sets for ruthenium atom [18] have been used together with the 6-31G** basis set for the first and second-row atoms [19]. The solvent correction is based on the Polarized Continuum Model (PCM) [20] with ε = 78.39 for water and ε = 36.64 for acetonitrile. This protocol has been validated for various Ru (II) complexes [21,9a,10]. The theoretical electronic vis/UV absorption spectra have been obtained by means of time-dependent DFT (TD-DFT) method [22] applying the solvent correction for water and acetonitrile. Eighty singlet states have been computed for each calculated TD-DDFT absorption spectrum. The calculations have been performed with the G03 quantum chemistry software [23].

3. Results and discussion

3.1. Synthesis and characterization

Among the library of available cyclometalated ruthenium compounds that are known to display interesting antitumor activity [6], we have chosen to study the electronic spectra of the compounds gathered in Chart 1 in more details. As some of us have already showed that **RDC11** and **RDC34** intercalate in DNA via the phenanthroline ligand [7], we have synthesized 2 new complexes, namely **RDC11Z** and **RDCbpZ** which derive from **RDC11** and **RDC34**, respectively, by substitution of the phenanthroline by the dipyrido [3,2-*a*:2′,3′-*c*]phenazine (dppz) ligand and the substitution of both phenanthroline by a dppz and a bipy ligand.

RDC11Z was synthesized according to our classical procedure [6b], i.e. via coordinating the dppz ligand on the tetrakis (acetonitrile) ruthenium (2-phenyl-2′-pyridine) cation. This led to the coordination of one of the nitrogen atoms of the dppz at the position trans to the carbon atom of the metalated 2-phenylpyridine ligand, in accordance with what had been found for corresponding reactions where dppz was replaced by either a 2,2′-bipyridine or a phenanthroline. The two remaining acetonitrile ligands on the new product could not be substituted by 2,2′-bipyridine to obtain **RDCbpZ**, thus we had to use a different strategy, analogous to the one reported recently [24], in order to obtain this compound. It required the synthesis, according to a procedure closely related to that described by D.A. Freedmann et al. [25], of Ru(2,2′-bipyridine)(dppz)Cl_2 followed by the cyclometalation of the 2-phenylpyridine ligand to obtain heteroleptic trischelate ruthenium derivatives. $[Ru(\eta^6\text{-}C_6H_6)Cl(\mu\text{-}Cl)]_2$ was first treated with 2,2′-bipyridine affording $[Ru(\eta^6\text{-}C_6H_6)(2,2'\text{-bipyridine})Cl]Cl$

Table 2
DFT(B3LYP) bond lengths (in Å) and bond angles (in °) calculated in vacuum, acetonitrile and water in **RDN34**, **RDC34**, **RDCbpZ** and **RDNbpZ** (vacuum and acetonitrile). When available the X-ray structures are reported for comparison.

	Vacuum	Acetonitrile[a]	Water	X-ray structure
RDN34 *bond lengths*				
Ru–N_2	2.113	2.105	2.106	–
Ru–N_3	2.111	2.101	2.101	–
Ru–N_4	2.113	2.105	2.105	–
Ru–N_5	2.111	2.101	2.101	–
Ru–N_6	2.099	2.089	2.089	–
Ru–N_7	2.099	2.089	2.089	–
Bond angles				
N_2–Ru–N_3	78.0	78.4	78.4	–
N_4–Ru–N_5	79.2	79.3	79.3	–
N_6–Ru–N_7	80.0	79.3	79.3	–
N_2–Ru–N_6	92.7	89.1	88.9	–
N_3–Ru–N_4	92.7	89.0	89.0	–
N_5–Ru–N_7	88.0	88.0	87.9	–
RDC34 *bond lengths*				
Ru–N_2	2.191	2.209 (2.182)	2.208	2.129
Ru–N_3	2.100	2.109 (2.087)	2.109	2.080
Ru–N_4	2.085	2.093 (2.069)	2.093	2.077
Ru–N_5	2.078	2.085 (2.061)	2.087	2.059
Ru–N_6	2.109	2.113 (2.100)	2.112	2.069
Ru–C_7	2.051	2.042 (2.046)	2.043	2.036
Bond angles				
N_2–Ru–N_3	77.7	77.3	77.4	78.8
N_4–Ru–N_5	79.4	79.2	79.1	79.8
N_6–Ru–C_7	79.3	79.3	79.3	79.3
N_2–Ru–N_4	90.3	89.6	89.5	88.7
N_5–Ru–C_7	89.5	90.1	89.8	94.1
N_6–Ru–N_3	89.4	89.3	89.3	90.7
RDCbpZ *bond lengths*				
Ru–N_2	2.115	2.113	2.113	2.089
Ru–N_3	2.109	2.108	2.110	2.061
Ru–N_4	2.082	2.085	2.086	2.042
Ru–N_5	2.209	2.203	2.201	2.126
Ru–N_6	2.090	2.094	2.094	2.040
Ru–C_7	2.044	2.043	2.043	2.055
Bond angles				
N_2–Ru–N_3	76.8	76.9	76.9	77.9
N_4–Ru–N_5	79.2	79.3	76.9	79.3
N_6–Ru–C_7	79.0	78.3	78.3	79.7
N_2–Ru–N_4	90.3	89.9	89.9	91.3
N_5–Ru–C_7	89.4	89.8	89.6	94.7
N_6–Ru–N_3	88.4	88.2	88.4	92.2
RDNbpZ *bond lengths*				
Ru–N_2	2.103	2.100	–	2.056
Ru–N_3	2.113	2.106	–	2.068
Ru–N_4	2.113	2.105	–	2.057
Ru–N_5	2.103	2.100	–	2.068
Ru–N_6	2.101	2.095	–	2.069
Ru–N_7	2.101	2.095	–	2.071
Bond angles				
N_2–Ru–N_3	88.4	88.2	–	87.5
N_4–Ru–N_5	88.4	88.2	–	87.1
N_6–Ru–N_7	89.3	88.7	–	92.7
N_2–Ru–N_4	96.8	96.3	–	96.7
N_5–Ru–N_7	77.9	78.2	–	79.8
N_6–Ru–N_3	96.3	96.6	–	93.4

[a] The values reported in parenthesis (**RDC34**) correspond to the bond lengths calculated with the PBE functional.

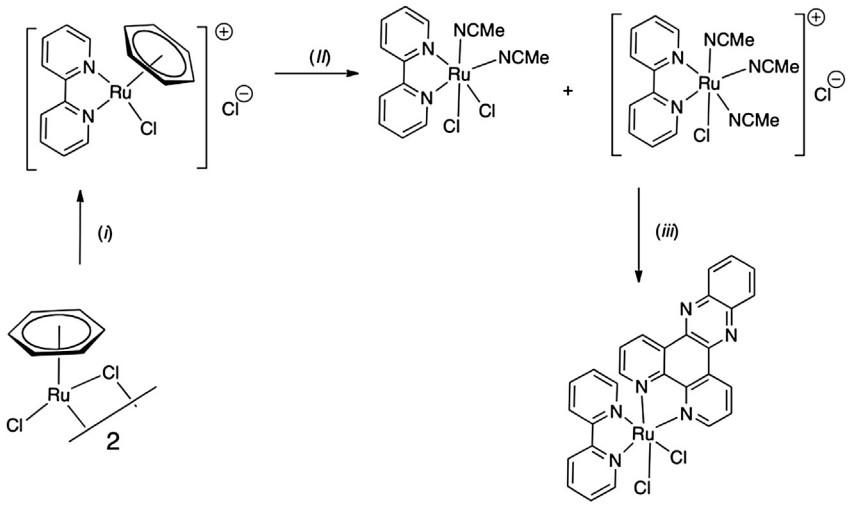

Scheme 1. Synthesis of Ru(bipy)(dppz)Cl_2. Reaction conditions : (*i*) 2,2′-bipyridine(2.1 eq.), CH_3CN, reflux 4 h; (*ii*) *hν*, 24 h. (*iii*) dipyridophenazine (1 eq.), acetone, reflux, 15 h.

(Scheme 1). The η^6-benzene ligand of this latter compound was then substituted by acetonitrile using a 400 W UV lamp to give a mixture of [Ru(2,2′-bipyridine)$(MeCN)_3$Cl]Cl and [Ru(2,2′-bipyridine)$(MeCN)_2Cl_2$]. This mixture, refluxed in acetone in the presence of dppz [26], led to the formation of [Ru(2,2′-bipyridine)(dppz)Cl_2]. Treating this latter compound with $AgPF_6$ and Ph-2-Py [27] in the presence of one equivalent of NMe_4OH, following a procedure described recently [6d], we obtained reasonable yields of [Ru(2,2′-bipyridine)(dppz)(2,2′-PhPy)]PF_6 in the form of a mixture of 2 compounds. Indeed, ^1H and ^{13}C NMR spectra yielded two sets of signals of unequal intensities which clearly reflected the presence of 2 isomers (2:1 ratio) that differ from each other by the position of the metalated carbon atom of the 2-phenylpyridine ligand with respect to the other ligands: in the one, it is *trans* to one N atom of the bipy while in the other it is *trans* to one N atom of the dppz ligand (Scheme 2). All our efforts to obtain each isomer in a pure form were vain as they both displayed very close behaviors in solution. Also, we were unable to obtain crystals for an X-ray diffraction analysis with this mixture of compounds. However, the corresponding OTf derivative, obtained by using AgOTf instead of $AgPF_6$, did afford mono crystals suitable for this kind of structure determination. We thus performed an X-ray diffraction study on one of these crystals, the detailed results of which are described in the next section. In short, we found that the isomer that had crystallized was the one having the carbon atom of the ortho-metalated phenyl ring *trans* to one N of the dppz ligand. We did not check whether all obtained crystals were equivalent to the one that was chosen for this study but it is likely that the second isomer crystallized also, since the physico-chemical properties of both compounds are very much the same as will be shown in the second part of this paper. In this context, we need to mention that a closely related compound in which the dppz ligand was substituted for a dppn ligand (dppn = benzo[*i*]dipyrido[3,2-*a*:2′,3′-*c*]phenazine) has been described very recently [28].

The synthesis of **RDNbpZ** (**5**) is detailed in the Supplementary material. All these compounds were fully characterized by different spectroscopies (NMR, mass and absorption spectroscopy) and X-Ray diffraction analysis. The details are reported in the Supplementary material for the newly synthesized cyclometalated complexes **RDC11Z** (**3**) and **RDCbpZ** (**4**) as well as for **RDNbpZ** (**5**).

3.2. Structural properties

RDCbpZ. The asymmetric unit of the crystallographic cell consists in 2 opposite enantiomers of Λ and Δ configurations, as they clearly are each other's mirror image. Analyzing one of these isomers, it is readily apparent that the cyclometalation of the 2-phenylpyridine has occurred as expected. Although the crystallographic evidence for the C atom identity vs. a N atom identity is scarce, the large influence this carbon atom has on the lengthening of the Ru–N bond *trans* to it ascertains to a degree our assignment (see Suppl. material). The rest of the structure does not deserve further comments as the geometric data, bond lengths and bond angles, are all within expected values.

RDNbpZ. Although this complex has been known for decades [29], it was surprising that no crystal structure had been reported for it to date. We have thus performed this determination in order to be able to compare the data to those of the geometric

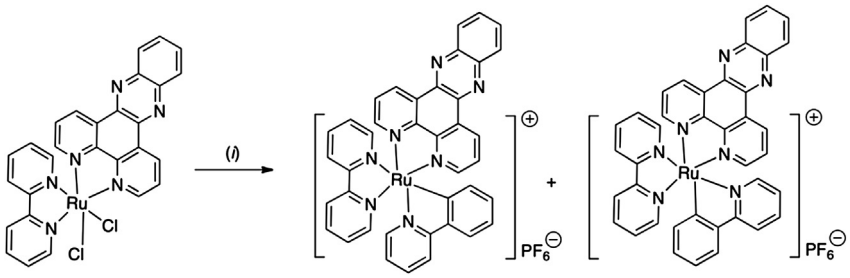

Scheme 2. Synthesis of two isomers of **RDCbpZ**, [Ru(bipy)(dppz)(2-Ph-2′-Py)]$^+PF_6^-$. Reaction conditions: (*i*) phenyl-2-pyridine (1 eq.), NMe_4OH (1 eq.), $AgPF_6$ (2 eq.), CH_2Cl_2, reflux, 24 h.

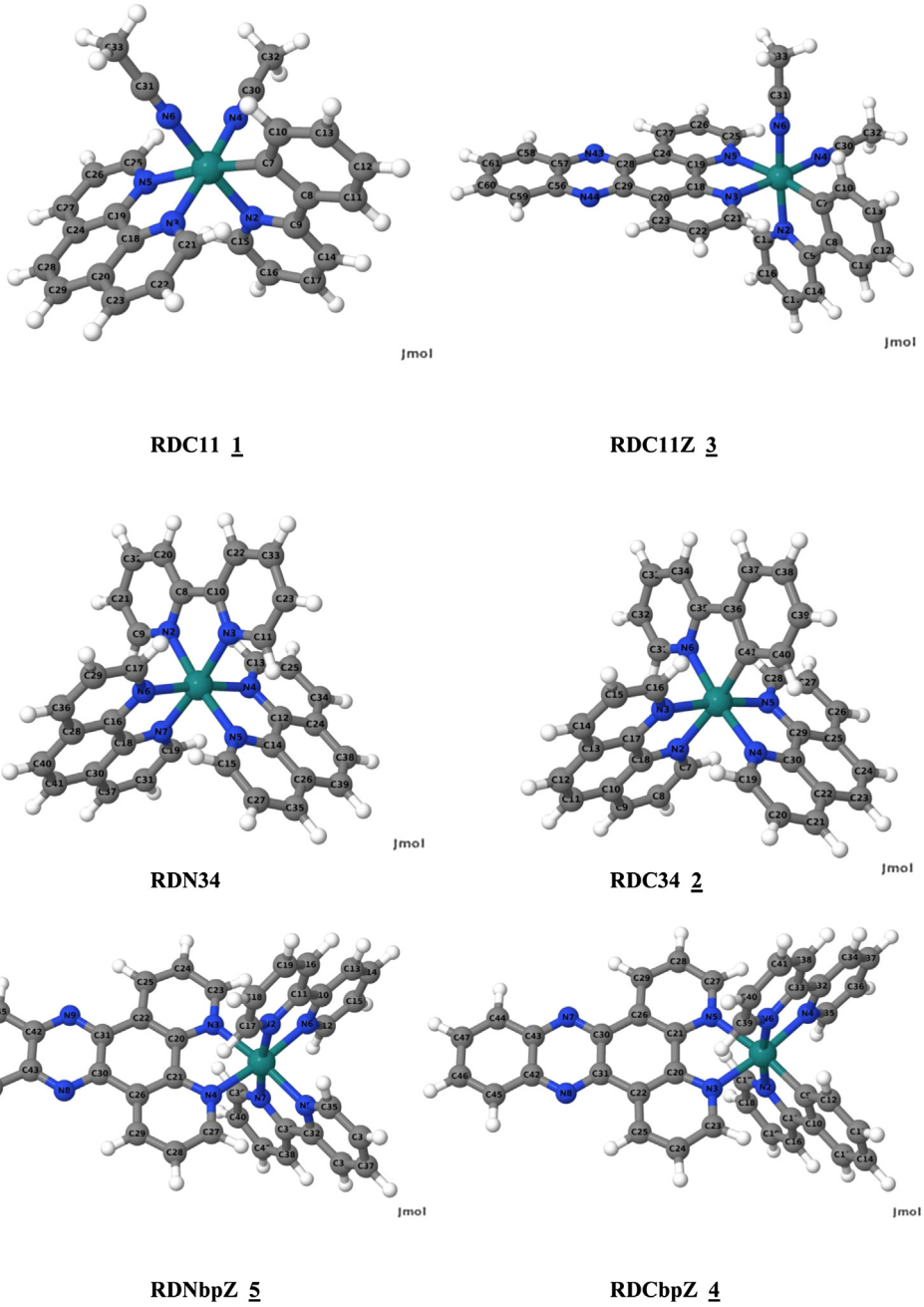

Fig. 1. DFT (B3LYP) optimized geometries of **1** $[Ru(MeCN)_2(phen)(PhPy)]^{1+}$ (**RDC11**), **2** $[Ru(phen)_2(PhPy)]^{1+}$ (**RDC34**), **3** $[Ru(MeCN)_2(PhPy)(dppz)]^{1+}$ (**RDC11Z**), **4** $[Ru(bpy)(PhPy)(dppz)]^{1+}$ (**RDCbpZ**), **5** $[Ru(bpy)_2(dppz)]^{1+}$ (**RDNbpZ**) and $[Ru(phen)_2(bpy)]^{2+}$ (**RDN34**).

optimization by DFT calculations, see below. However, it turned out that the structural parameters of **RDNbpZ** were remarkably close to those reported for many related molecules (we found 8 closely related molecules characterized by X-ray diffraction studies) [30]. Thus our structural data are reported in the Supplementary material.

The optimized geometries of the six complexes are depicted in Fig. 1 and the corresponding calculated bond distances and angles are reported in Tables 2 and 3. For **RDC34**, **RDCbpZ**, and **RDNbpZ** the experimental data are reported for comparison. The optimized geometry of the dicationic reference complex $[Ru(phen)_2(bpy)]^{2+}$ (**RDN34**) is reported in Table 2.

The global structures of **RDC34** and **RDN34** are very similar despite the substitution of one nitrogen atom by a carbon atom in **RDC34**. As expected we observe a shortening of the Ru–C_7 bond as compared to the Ru–N_7 bond (2.051 Å vs. 2.10 Å) but we also observe a 3.7% elongation of the Ru–N_2 bond trans to the Ru–C_7 bond.

The optimized structures of the NO_2Phpy and NH_2Phpy substituted complexes **RDC40** and **RDC41** are very similar to the one of **RDC34** (see Supplementary material). The theoretical trends agree rather well with the experimental observations. The solvent corrections are very small, give similar values in water and acetonitrile and never exceed 0.5% within the present model. For the fully nitrogen substituted compound **RDN34** the Ru–N bond lengths are shortened by the solvent correction whereas the Ru–N bonds are elongated in **RDC34** due to a shortening of the Ru–C_7 bond by 0.01 Å. While the theoretical bond angles are in excellent

Table 3
DFT(B3LYP) bond lengths (in Å) and bond angles (in °) calculated in vacuum, acetonitrile and water in RDC11 and RDC11Z.

	Vacuum	Acetonitrile	Water
RDC11 *bond lengths*			
$Ru-N_2$	2.223	2.217	2.219
$Ru-N_3$	2.104	2.105	2.106
$Ru-N_4$	2.031	2.030	2.032
$Ru-N_5$	2.020	2.022	2.023
$Ru-N_6$	2.106	2.104	2.104
$Ru-C_7$	2.050	2.045	2.044
Bond angles			
N_2-Ru-N_3	77.3	77.5	77.5
N_4-Ru-N_5	90.5	90.4	90.5
N_6-Ru-C_7	79.4	79.5	79.5
N_2-Ru-N_4	89.1	88.5	88.3
N_5-Ru-C_7	88.7	89.6	89.9
N_6-Ru-N_3	90.2	90.4	90.4
RDC11Z *bond lengths*			
$Ru-N_2$	2.219	2.211	2.211
$Ru-N_3$	2.104	2.103	2.104
$Ru-N_4$	2.028	2.032	2.033
$Ru-N_5$	2.019	2.022	2.023
$Ru-N_6$	2.110	2.104	2.105
$Ru-C_7$	2.047	2.045	2.045
Bond angles			
N_2-Ru-N_3	77.1	77.1	77.1
N_4-Ru-N_5	90.6	90.0	90.5
N_6-Ru-C_7	79.4	79.5	79.5
N_2-Ru-N_4	89.1	88.5	88.4
N_5-Ru-C_7	88.6	89.3	89.7
N_6-Ru-N_3	90.2	90.5	90.5

agreement with the X-ray structures, the theoretical bond distances are systematically slightly overestimated with respect to the experimental values but reproduce the trends and global structure very well.

The substitution of a phen ligand in **RDC34** by the dipyridophenazine dppz ligand does not disturb drastically the structure of the complex **RDCbpZ**. The Ru–N bonds of the dppz ligand are slightly elongated with respect to the phen whereas the $Ru-C_7$ bond length in *trans* to the dppz is shortened. As observed for **RDC34** and **RDN34**, the theoretical geometries are not very sensitive to the solvent corrections.

The calculated bond lengths and bond angles of **RDC11** and **RDC11Z** are reported in Table 3. The X-ray structures of these molecules are not available.

Similarly to **RDC34** and **RDCbpZ** the $Ru-N_2$ bond *trans* to the C_7 atom is drastically elongated to 2.22 Å. The $Ru-C_7$ bond length of ~2.05 Å is now comparable to the strong $Ru-NCCH_3$ bond lengths calculated at ~2.02–2.03 Å. The solvent corrections are nearly negligible. The same trends are observed in **RDC11Z** where the elongation of the $Ru-N_2$ bond is slightly attenuated by the presence of the dppz ligand.

The calculated geometries of the investigated complexes point to a rather rigid structure whatever the environment is. The calculated bond lengths are appreciably overestimated as they usually are with the B3LYP functional [31]. The use of the BPE functional leads to calculated bond length very similar to the one obtained with the B3LYP functional as illustrated by the values reported in Table 2 for **RDC34**. The introduction of a strong Ru–C bond has a minor effect on the coordination sphere around the metal atom (**RDC34** vs. **RDN34**) keeping the Ru–N bond lengths and bond angles similar, the only noticeable alteration being an increase of the $Ru-N_2$ bond *trans* to the Ru–C bond. This $Ru-N_2$ elongation is even more dramatic in the CH_3CN substituted complexes (**RDC11** and **RDC11Z**) where two additional strong $Ru-NCCH_3$ bonds enhance this electronic effect. Whereas the polypyridyl complex **RDN34** shows a totally localized electronic structure with the $4d_{Ru}$ orbitals being the HOMO, HOMO − 1 and HOMO − 2 and the LUMO, LUMO + 1, LUMO + 2 and LUMO + 3 corresponding to the π^*_{bpy} and π^*_{phen} orbitals, the organometallic complexes **RDC34**, **RDCbpZ**, **RDNbpZ**, **RDC11** and **RDC11Z** point to a significant delocalization of the electronic density between the metal center and the phenyl-pyridine ligand as it is illustrated (Scheme 3) for **RDN34** and **RDC34**.

3.3. Electronic absorption spectroscopy

The experimental absorption spectra of the cyclometalated complexes **RDC34**, **RDC40**, **RDC41**, **RDCbpZ**, **RDC11**, and **RDC11Z** recorded in acetonitrile and depicted in Figs. 2–4 are characterized by an intense band centered at 270 nm corresponding to a strong absorption of the intra-ligand (IL) excited states and a weak absorption around 370 nm. This shoulder is more intense in the dppz-substituted complexes (**RDCbpZ**, **RDNbpZ**, **RDC11Z**) and is hardly detected in **RDN34**. The tail of the visible band extending towards 650 nm is another characteristic of the cyclometalated complexes that absorb between 550 nm and 400 nm in the low-lying metal-to-ligand-charge-transfer (MLCT) excited states. The visible band

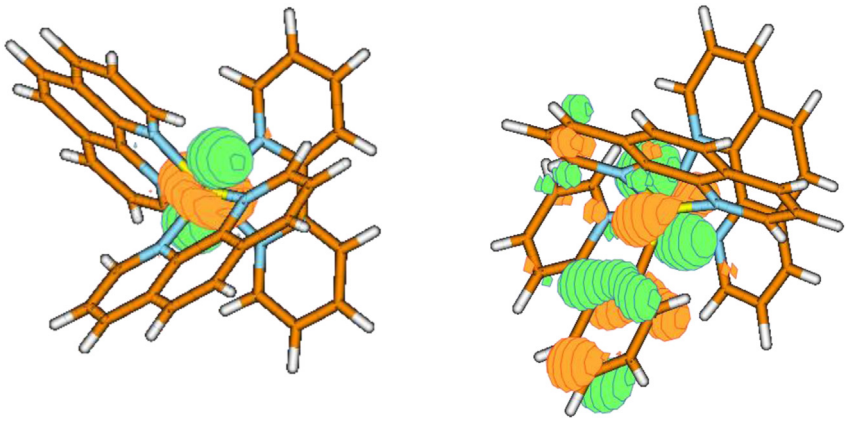

Scheme 3. Kohn–Sham HOMO orbitals describing the metal–ligand interactions in **RDN34** (a) and **RDC34** (b).

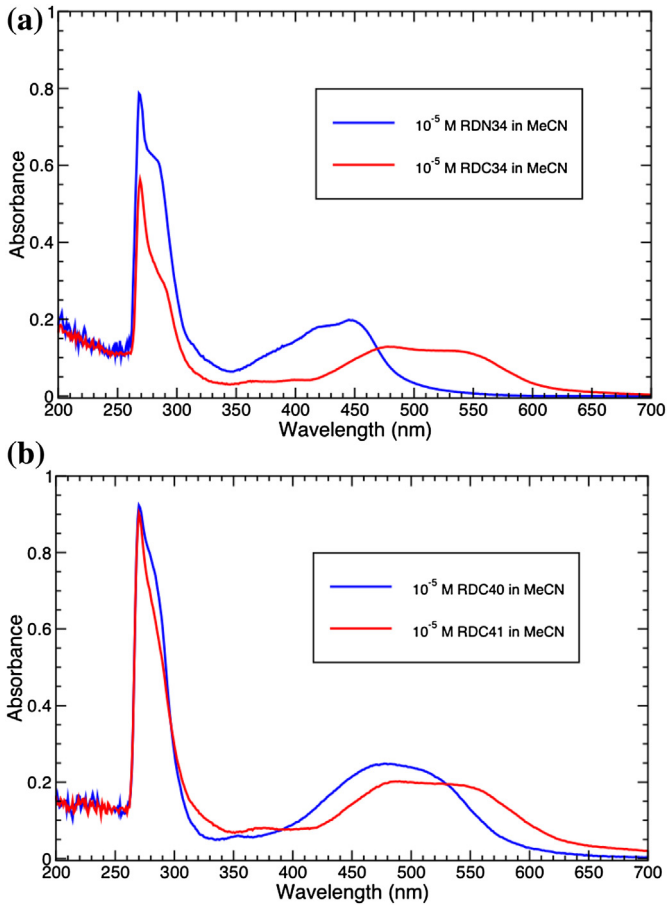

Fig. 2. Experimental absorption spectra of a) **2** $[Ru(phen)_2(PhPy)]^{1+}$ (**RDC34**) and $[Ru(phen)_2(bpy)]^{2+}$ (**RDN34**); b) **6** $[Ru(phen)_2(NO_2PhPy)]^{1+}$ (**RDC40**) and **7** $[Ru(phen)_2(NH_2PhPy)]^{1+}$ (**RDC41**) recorded in acetonitrile.

maximum is red shifted in **RDC34**, **RDC40**, **RDC41** and **RDCbpZ** with respect to the polypyridinic analogs **RDN34** and **RDNbpZ**.

As illustrated by previous theoretical studies performed on Ru (II) polypyridyl complexes, the theoretical spectra of this class of molecules are characterized by a high density of electronic states in the visible/UV energy domain, a large mixing between MLCT/IL and ligand-to-ligand-charge-transfer (LLCT) states in the upper part of the spectrum and a significant sensitivity to the environment of the IL states localized on the dppz ligand [9a,10].

The solvent corrected TD-DFT transition energies (in CH_3CN) of the low-lying excited states of the four investigated complexes are reported in Table 4 (**RDC34**, **RDCbpZ**) and Table 5 (**RDC11** and **RDC11Z**). The details of the one-electron excitations in the main configuration are given in Tables S1, S2 and S3 (**RDC40**, **RDC41**) of the Supplementary material. The main experimental absorption bands are reported for comparison, as well as the theoretical spectra of **RDN34** and **RDNbpZ** (Table 4), the polypyridyl complexes of reference.

The theoretical absorption spectra of the investigated complexes are represented in Figs. 5–7 assuming a Gaussian inhomogeneous broadening of 2000 cm^{-1} (FWHM) for each computed electronic transition in order to roughly reproduce the appearance of the experimental absorption bands.

The absorption spectra of the RDC complexes are red shifted with respect to those of the RDN complexes with a tail between 500 nm and 600 nm assigned to low-lying $MLCT_{phen}$ and $MLCT_{dppz}$ in the dppz-substituted complex **RDCbpZ**. This extension to the red is also observed in **RDC11Z** with contributions of $MLCT_{dppz}$ transitions.

The theoretical spectrum of **RDC34** (Fig. 5a) exhibits a large band between 545 nm and 420 nm corresponding mainly to $MLCT_{phen}$ transitions with one intense peak centered at 496 nm (Scheme 4a).

These features reflect the main characteristics of the experimental spectrum measured in CH_3CN. The upper $MLCT_{phen}$ states are contaminated by $MLCT_{Phpy}$ and MC contributions. The shoulder observed at 362 nm is attributed to a mixed $MLCT_{Phpy}$/MC/$MLCT_{pyPh}$ state calculated at 369 nm (Scheme 4b). The upper part of the theoretical spectrum of **RDC34** starts at 287 nm slightly blue shifted with respect to the experimental one (307 nm) with a series of IL states localized either on Phpy (287 nm) (Scheme 4c) or on the phen ligand (265 nm). These transitions contribute to the intense absorptions observed at 285 nm and 270 nm. Other IL_{phen} and IL_{Phpy} states contribute to an intense band around 250 nm not detected experimentally. Whereas the addition of an amino group NH_2 to the Phpy ligand (**RDC41**) does not modify the electronic spectroscopy (except for a small red shift of the visible band with respect to **RDC34** due to an increase in π_{Phpy} character of the HOMO), the nitro group NO_2 (**RDC40**) induces a more significant perturbation (Fig. 5b). Indeed, the lowest $MLCT_{phen}$ excited states are

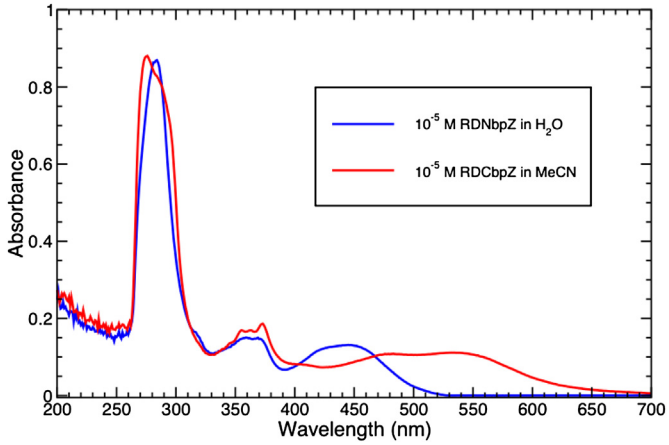

Fig. 3. Experimental absorption spectra of **4** $[Ru(bpy)(PhPy)(dppz)]^{1+}$ (**RDCbpZ**) recorded in acetonitrile and **5** $[Ru(bpy)_2(dppz)]^{2+}$ (**RDNbpZ**) recorded in water.

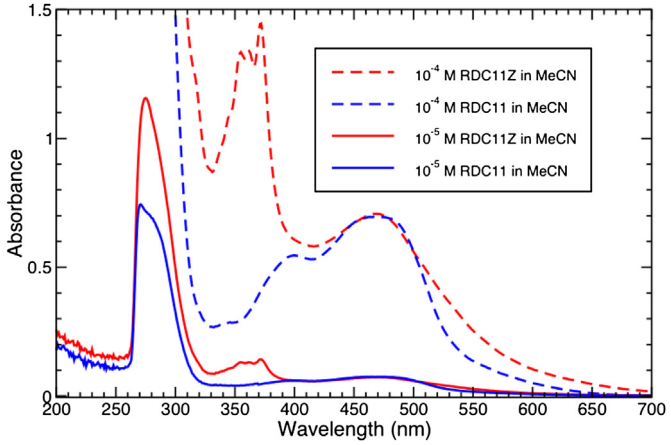

Fig. 4. Experimental absorption spectra of **1** $[Ru(MeCN)_2(phen)(PhPy)]^{1+}$ (**RDC11**), and **3** $[Ru(MeCN)_2(PhPy)(dppz)]^{1+}$ (**RDC11Z**) recorded in various concentrations of acetonitrile.

Table 4
Solvent corrected (CH_3CN) TD-DFT transition energies (in nm and eV) of the low-lying singlet excited states of **RDC34**, **RDN34**, **RDCbpZ** and **RDNbpZ** with significant oscillator strengths (all excited states are reported in Table S1 of Supplementary material).

Complex exp. bands	Character	nm	eV	*f*
RDC34				
544	$MLCT_{phen}$	545	2.28	0.014
480	$MLCT_{phen}$	496	2.50	0.17
	$MLCT_{phen}$	477	2.60	0.05
	$MLCT_{phen}$	464	2.67	0.04
	$MLCT_{phen}$	458	2.71	0.07
	$MLCT_{phen}/MLCT_{Phpy}/MC$	447	2.77	0.03
	$MLCT_{phen}/MLCT_{Phpy}/MC$	438	2.83	0.07
362	**$MLCT_{Phpy}$**/MC/$MLCT_{pyPh}$	369	3.36	0.07
285	$LLCT_{Phpyphen}/MLCT_{phen}/IL_{Phpy}/IL_{phen}$	287	4.31	0.06
	$IL_{Phpy}/LLCT_{Phpyphen}/IL_{phen}$	287	4.32	0.12
270	IL_{phen}	265	4.68	0.15
	IL_{phen}	260	4.76	0.03
	IL_{phen}	258	4.81	0.38
	$IL_{phen}/LLCT_{PhpypyPh}$	256	4.85	0.80
	$MLCT_{phenpy}/MC/IL_{Phpy}$	253	4.90	0.032
	IL_{Phpy}	250	4.96	0.24
RDN34				
450	$MLCT_{bpy}/MLCT_{phen}$	442	2.80	0.022
	$MLCT_{bpy}/MLCT_{phen}$	439	2.82	0.020
	$MLCT_{phen}/MLCT_{bpy}$	427	2.90	0.045
	$MLCT_{phen}/MLCT_{bpy}$	426	2.91	0.088
	$MLCT_{bpy}/MLCT_{phen}$	423	2.93	0.1
	$MLCT_{phen}$	410	3.02	0.077
	$MLCT_{phen}$	395	3.14	0.074
	$MLCT_{bpy}$	312	3.97	0.0642
290	$IL_{bpy}/MLCT_{phen}/LLCT_{bpy}$	281	4.41	0.22
	$MC/MLCT_{phen}/IL_{bpy}$	280	4.43	0.146
270	IL_{phen}	268	4.63	0.096
	$IL_{phen}/MLCT_{phen}$	265	4.68	0.112
	$IL_{phen}/LLCT_{bpy}$	262	4.73	0.30
	$IL_{phen}/LLCT_{bpy}$	260	4.77	1.025
RDCbpZ				
555	$MLCT_{dppz}$	577	2.15	0.019
	$MLCT_{dppz}$	545	2.28	0.026
476	$MLCT_{bpy}/MLCT_{dppz}$	503	2.46	0.142
	$MLCT_{dppz}/MLCT_{bpy}/MC/IL_{phpy}$	455	2.72	0.119
	$MLCT_{dppz}$	436	2.84	0.077
370	$MLCT_{bpy}/MLCT_{phpy}$	376	3.30	0.067
350	$/IL_{dppz}/LLCT_{dppz}$	340	3.65	0.202
	$MLCT_{dppz}/LLCT_{dppz}/IL_{dppz}/IL_{bpy}$	294	4.22	0.146
	$LLCT_{dppz}/IL_{dppz}$	288	4.30	0.063
289	$IL_{dppz}/MLCT_{dppz}/LLCT_{dppz}$	287	4.32	0.729
	$IL_{phpy}/IL_{dppz}/MLCT_{dppz}$	287	4.33	0.691
	$MLCT_{dppz}/MLCT_{phen}$	284	4.37	0.081
	$LLCT_{bpy}/IL_{bpy}/IL_{phpy}$	281	4.41	0.093
273	$IL_{bpy}/LLCT_{bpy}$	277	4.48	0.26
	$MLCT_{bpy}/MLCT_{dppz}/MC/LLCT_{dppz}/IL_{dppz}/IL_{phpy}$	275	4.51	0.086
	$IL_{dppz}/MLCT_{bpy}/MLCT_{dppz}$	259	4.79	0.247
	$IL_{phpy}/MC/MLCT_{phpy}$	258	4.81	0.050
RDNbpZ				
454	$MLCT_{dppz}/MLCT_{bpy}$	453	2.74	0.10
430	$MLCT_{bpy}/MLCT_{dppz}$	415	2.98	0.124
	$MLCT_{bpy}/MLCT_{dppz}$	412	3.01	0.13
375	$MLCT_{dppz}$	370	3.35	0.06
	$MLCT_{dppz}/IL_{dppz}$	369	3.36	0.046
350	IL_{dppz}	338	3.66	0.15
320	$MLCT_{bpy}$	310	3.99	0.06
290	$IL_{dppz}/MLCT_{bpy}$	296	4.18	0.87
	$IL_{dppz}/LLCT_{bpy}/Il_{bpy}/MLCT_{dppz}$	292	4.25	0.34
	$Il_{bpy}/MLCT_{bpy}/IL_{dppz}$	**290**	**4.27**	**0.12**
270	$IL_{bpy}/LLCT_{dppz}/MLCT_{bpy}$	279	4.45	0.29
	$IL_{bpy}/LLCT_{dppz}/MLCT_{bpy}$	277	4.48	0.61
	$MLCT_{dppz}$	272	4.55	0.097
	$LLCT_{bpy}/IL_{dppz}$	266	4.66	0.1
	$IL_{dppz}/MLCT_{dppz}$	263	4.72	0.13
	$MLCT_{dppz}/IL_{dppz}$	260	4.78	0.193
	$MLCT_{dppz}$	253	4.89	0.108

destabilized by the presence of low-lying $MLCT_{NO2}$ due to the stabilization of the π^* of this group in acetonitrile. The occurrence of an intense peak at 490 nm in the spectrum of **RDC40** (Fig. 2b) illustrates this effect. The TD-DFT results obtained for **RDC40** and **RDC41** are detailed in Table S3.

When replacing the Phpy ligand (**RDC34**) by a bpy ligand (**RDN34**) (Fig. 5a) two important differences are observed: i) a significant blue shift (~100 nm) of the visible part of the spectrum accompanied by a large mixing between the $MLCT_{phen}$ and $MLCT_{bpy}$ states in **RDN34**; ii) the disappearance of the double $MLCT_{phen}$ peak structure observed in **RDC34** replaced by a single intense absorption at 423 nm corresponding to a mixed $MLCT_{bpy}/MLCT_{phen}$ transition.

The short wavelength parts of the spectra for **RDC34** and **RDN34** (Fig. 5a) are nearly identical with two sets of intense bands centered at ~280 nm and ~260 nm. However, in the case of **RDN34**, IL states that were nearly pure in **RDC34** are now contaminated by MLCT, MC and LLCT contributions.

The theoretical absorption of **RDNbpZ** (Fig. 6) can be compared to that of **RDN34** (Fig. 5a). The presence of the dppz π acceptor ligand is responsible for a modest shift to the red, especially in the UV energy domain. Indeed, two intense IL peaks observed at ~280 nm and ~260 nm in **RDN34** are shifted to ~290 nm and ~278 nm in **RDNbpZ** and can be attributed to IL_{bpy} transitions with contributions of $LLCT_{dppz}$ and $MLCT_{bpy}$ states. An additional shoulder appears at ~260 nm in the theoretical spectrum of **RDNbpZ** due to the presence of intense IL_{dppz} and $MLCT_{dppz}$ transitions. Instead of $MLCT_{bpy}/MLCT_{phen}$ mixing observed in **RDN34**,

Table 5
Solvent corrected (CH_3CN) TD-DFT transition energies (in nm and eV) of the low-lying singlet excited states of **RDC11** and **RDC11Z** with significant oscillator strengths (the whole theoretical absorption spectra are reported in Table S2 of Supplementary material).

Complex exp. bands	Character	nm	eV	*f*
RDC11				
480	$LLCT_{CNphen}/MLCT_{phen}$	465	2.66	0.011
455	$MLCT_{phen}/LLCT_{CNphen}$	441	2.81	0.13
390	$MLCT_{Phpy}/LLCT_{Phpy}/IL_{Phpy}$	361	3.44	0.052
	$MLCT_{Phpy}/IL_{Phpy}/LLCT_{phen}$	353	3.51	0.051
290	$IL_{Phpy}/MC/MLCT_{CN}/IL_{CN}$	288	4.31	0.121
	$IL_{CN}/MLCT_{CN}/MC$	264	4.69	0.128
	$MLCT_{CN}/MC/IL_{CN}/IL_{phen}/LLCT_{CN}$	263	4.72	0.041
	$IL_{Phpy}/IL_{phen}/MLCT_{Phpy}/MLCT_{CN}/IL_{CN}$	261	4.75	0.19
	$MLCT_{CN}/LLCT_{CN}/IL_{phen}/MLCT_{phen}/IL_{Phpy}/MC/IL_{CN}$	260	4.78	0.118
	$MC/MLCT_{Phpy}/IL_{Phpy}/MLCT_{CN}/IL_{CN}/LLCT_{CN}$	258	4.81	0.078
	$MLCT_{phen}/IL_{phen}/MLCT_{CN}/MC/IL_{CN}$	256	4.83	0.253
	$MLCT_{CN}/MC/IL_{CN}/MLCT_{Phpy}/IL_{Phpy}$	251	4.93	0.09
	$LLCT_{phen}/LLCT_{Phpy}/MLCT_{Phpy}/IL_{Phpy}$	248	5.00	0.097
RDC11Z				
475	$MLCT_{dppz}$	533	2.32	0.021
	$MLCT_{dppz}$	510	2.43	0.012
430	$MLCT_{dppz}$	455	2.72	0.051
	$MLCT_{dppz}$	432	2.86	0.139
380	$MLCT_{Phpy}/IL_{Phpy}$	347	3.57	0.057
352	$LLCT_{dppz}/MLCT_{dppz}/IL_{dppz}$	339	3.66	0.212
275	$MLCT_{dppz}/LLCT_{dppz}$	298	4.16	0.071
	$LLCT_{dppz}/MLCT_{dppz}/MLCT_{dppz}$	294	4.21	0.051
	$IL_{Phpy}/LLCT_{dppz}/MLCT_{dppz}$	288	4.30	0.35
	$IL_{dppz}/IL_{Phpy}/MC/MLCT_{CN}$	287	4.31	1.08
	$MC/MLCT_{CN}/MLCT_{dppz}/MLCT_{Phpy}$	285	4.35	0.1264
	$IL_{Phpy}/MLCT_{dppz}/LLCT_{dppz}/MLCT_{Phpy}/MLCT_{CN}$	259	4.78	0.0954
	$MLCT_{CN}/IL_{Phpy}/MC$	259	4.78	0.0179
	ILdppz/$LLCT_{dppz}/MLCT_{dppz}$	258	4.80	0.3268
	IL_{dppz}	256	4.84	0.0409

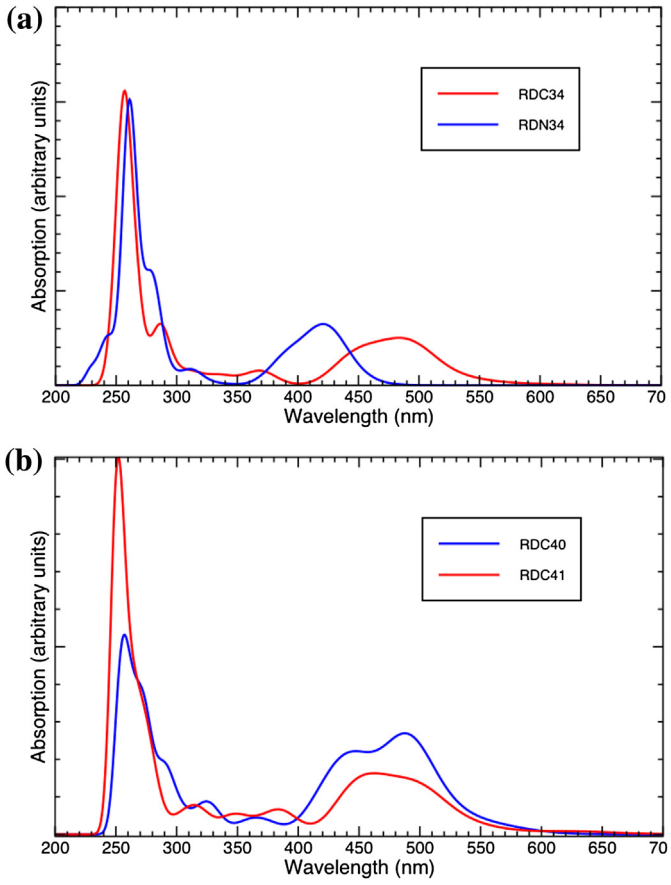

Fig. 5. TD-DFT theoretical absorption spectra with solvent correction (acetonitrile) of a) **2** $[Ru(phen)_2(PhPy)]^{1+}$ (**RDC34**) and $[Ru(phen)_2(bpy)]^{2+}$ (**RDN34**); b) **6** $[Ru(phen)_2(NO_2PhPy)]^{1+}$ (**RDC40**) and **7** $[Ru(phen)_2(NH_2PhPy)]^{1+}$ (**RDC41**).

the spectrum of the dppz substituted analog shows large $MLCT_{dppz}$/$MLCT_{bpy}$ mixing in the visible energy domain with three intense absorptions at 453 nm, 415 nm and 412 nm contributing to the large band between 500 nm and 400 nm. The presence of a shoulder at 350 nm is characteristic of the dppz complexes and corresponds to the IL_{dppz} transition.

The experimental spectrum of **RDNbpZ** is well reproduced by the TD-DFT calculations and can be interpreted unequivocally. The visible band between 500 nm and 400 nm is assigned to the lowest $MLCT_{dppz}$/$MLCT_{bpy}$ transitions. The shoulder at ~375 nm corresponds to a pure $MLCT_{dppz}$ state calculated at 370 nm. The intense absorption bands observed between 300 nm and 260 nm cover the series of IL, MLCT and LLCT transitions localized on the bpy and dppz ligands and calculated between 296 nm and 253 nm. The small peak at 320 nm corresponds to one pure $MLCT_{bpy}$ state and the absorption at 350 nm to the IL_{dppz} transition.

Whereas the comparison between the theoretical spectra of **RDN34** and **RDNbpZ** is straightforward this is not the case for **RDC34** (Fig. 5a) and **RDCbpZ** (Fig. 6). However we can extract similar trends. Both spectra are characterized by a double peak absorption in the visible energy domain calculated at 503 nm and 455 nm in **RDCbpZ**. Again the presence of bpy and dppz ligands in **RDCbpZ** introduce large mixings among the low-lying MLCT states as pointed out for **RDN34** and **RDNbpZ**. **RDCbpZ**, as the other dppz substituted complexes, presents a shoulder centered at ~350 nm that does not appear in **RDC34** and **RDN34**. This absorption has also been observed in other ruthenium dppz complexes [11] and corresponds to an IL_{dppz} transition. This state may play an important role in reversible electron transfer processes when the complex is intercalated in DNA for instance [32,11]. In the case of **RDCbpZ** this state is not pure and is altered by LLCT from Phpy to dppz.

The presence of various IL states, namely IL_{phen}, IL_{Phpy}, IL_{bpy} and IL_{dppz} in the upper part of the spectra of the four complexes leads to very similar features with two series of strong absorptions around 290 nm nd 270 nm blue shifted to 280 nm and 260 nm in **RDN34** by the combination of the bpy and phen ligands.

The results obtained for **RDNbpZ** and **RDCbpZ** (Fig. 6) are in line with those reported recently for $[Ru(bpy)_2dppn]^{2+}$ and [Ru(Phpy)(bpy)dppn]$^{+}$ (dppn = benzo[*i*]dipyrido[3,2-*a*:2′,3′-*c*]phenazine) with a modest red shift of the lowest MLCT states localized on the dppn ligand with respect to the $MLCT_{bpy}$ states. Similarly to the systems investigated here, the cyclometalated $Phpy^{-}$ substituted Ru (II) complexes show an important red shift of ~100 nm of the MLCT transition when compared to the conventional polypyridyl compounds [28].

Table 5 reports the solvent corrected (CH3CN) TD-DFT transition energies of the most important low-lying singlet excited states of **RDC11** and **RDC11Z**. The complete theoretical spectra are reported in Table S2. The theoretical spectra of the CN groups substituted complexes do not differ drastically from the one reported for **RDC34** and **RDCbpZ** in Table 4. In agreement with the experimental data the start of the absorption spectrum of **RDC11** is blue shifted at

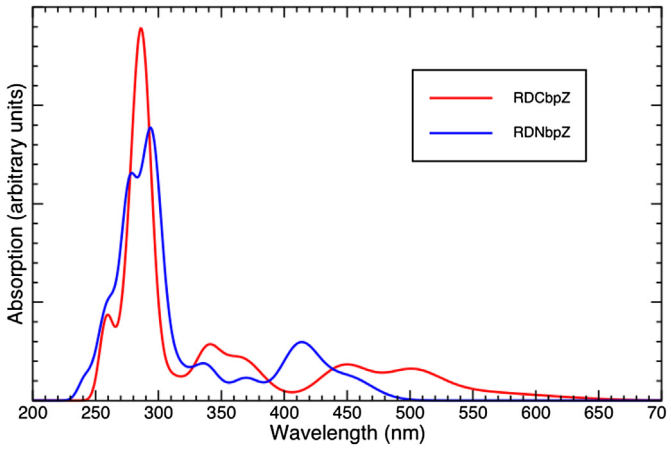

Fig. 6. TD-DFT theoretical absorption spectra with solvent correction (acetonitrile) of **4** $[Ru(bpy)(PhPy)(dppz)]^{1+}$ (**RDCbpZ**) and **5** $[Ru(bpy)_2(dppz)]^{2+}$ (**RDNbpZ**).

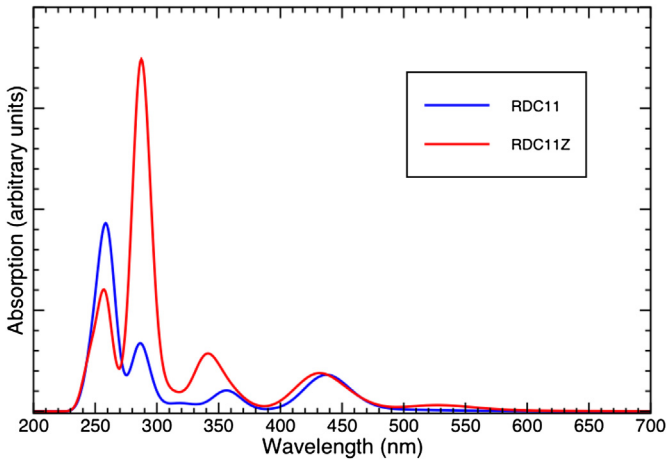

Fig. 7. TD-DFT theoretical absorption spectra with solvent correction (acetonitrile) of **1** $[Ru(MeCN)_2(phen)(PhPy)]^{1+}$ (**RDC11**) and **3** $[Ru(MeCN)_2(PhPy)(dppz)]^{1+}$ (**RDC11Z**).

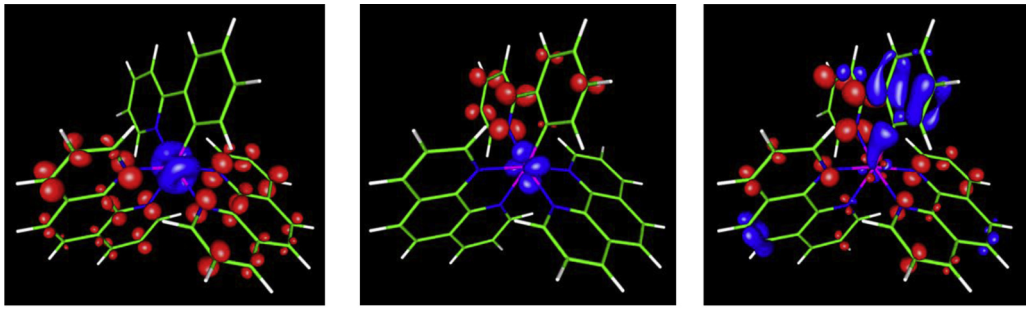

Scheme 4. **RDC34** electronic density variation associated to the (a) $MLCT_{phen}$ transition calculated at 496 nm ($f = 0.1725$), (b) mixed $MLCT_{Phpy}$/MC/$MLCT_{pyPh}$ transition calculated at 369 nm ($f = 0.0662$) and (c) IL_{Phpy}/$LLCT_{Phpyphen}$/IL_{phen} transition calculated at 287 nm ($f = 0.1158$) (in blue decrease of density, in red increase of density). (For interpretation of the references to color in this scheme legend, the reader is referred to the web version of this article.)

465 nm with respect to the one of **RDC34** (545 nm) but the UV parts of the two complexes are very similar. In contrast to **RDC34** identified by pure low-lying $MLCT_{phen}$ states, significant contributions of LLCT from the CN groups to the phen ligand characterize the visible part of the spectrum of **RDC11**. The blue shift may be attributed to this LLCT/MLCT mixing. Similarly to the experimental spectrum, the theoretical spectrum of **RDC11** is distinguished by a double shoulder between 400 nm and 500 nm (Fig. 4) with an intense band calculated at 441 nm corresponding to a $MLCT_{phen}$/$LLCT_{CNphen}$ transition and another one centered at 357 nm. The intense peak observed at 290 nm is attributed to the next transitions calculated at 288 nm and 264 nm and corresponding to IL_{Phpy} and IL_{CN} with strong oscillator strengths.

The substitution of the phen ligand in **RDC11** by a dppz ligand in **RDC11Z** leads to a red shift of the visible absorption that starts at 533 nm and is followed by several shoulders calculated at 455 nm, 432 nm, 347 nm and 339 nm slightly blue-shifted with respect to the experimental bands detected at 475 nm, 430 nm, 375 nm and 352 nm. Similarly to the other dppz substituted complexes the visible part of the spectrum of **RDC11Z** is dominated by $MLCT_{dppz}$ transitions until the peak at 430 nm. In absence of bpy ligand there is no mixing like in **RDCbpZ** and **RDNbpZ**. The first $MLCT_{Phpy}$ state is calculated at 347 nm, as compared to 447 nm in **RDC34**, with moderate oscillator strength. In the experimental spectrum of **RDC11Z** an intense peak is observed at ~275 nm. This solvent dependent band, the intensity of which increases dramatically in water, is attributed to strong transitions calculated at 287 nm and 258 nm of mixed characters but predominantly IL_{dppz}. The IL_{Phpy} transitions present in the same region of the absorption spectrum are less intense.

Surprisingly, and within the limits of the present method, the RDC complexes absorption spectra are not perturbed by the presence of low-lying MC reactive excited states. Their contributions are minor in the visible part of the spectra of **RDC34** and **RDCbpZ** and in the UV part of **RDC11**. The first significant MC transition occurs at 285 nm in **RDC11Z** and is mixed with $MLCT_{CN}$, $MLCT_{dppz}$ and $MLCT_{Phpy}$.

4. Conclusion

The synthesis of new complexes considered as interesting anticancer drugs candidates with dppz ligands, optimal for intercalation in DNA, has been realized. It has been shown that the structural properties of the RDC and RDN analogs are very similar despite the substitution of one nitrogen atom by a carbon atom. As expected, a shortening of the Ru–C bond as compared to the Ru–N bond and an elongation of the Ru–C bond (>3%) are observed. The Ru–N bond of the dppz substituted complexes are slightly elongated with respect to the phen and the Ru–C bond *trans* to dppz is shortened. These trends are well reproduced by theory eventhough calculated bond distances are systematically overestimated with respect to the experimental data, a general feature of DFT (B3LYP) calculations. The theoretical geometries are not drastically affected by the solvent correction and point to rather rigid structures. In contrast to polypyridyl RDN complexes where the electronic structure is totally localized either on $4d_{Ru}$ or on the low-lying π^*_{bpy}, the organometallic RDC complexes point to an important delocalization of the electronic density between the metal atom and the phenyl-pyridine ligand. This characteristic may have consequences on the photoreactivity of these complexes.

The absorption spectra of the RDC are very similar with an intense peak centered at 270 nm, a shoulder at about 370 nm, more intense in dppz substituted complexes, and a visible band between 550 and 400 nm characterized by a long tail until 650 nm. The maximum of the visible band is red shifted in the RDC compounds with respect to the spectrum observed for the conventional polypyridyl analogs. The calculations reproduce these observed trends well.

From a detailed analysis of the theoretical spectra of the series of complexes under investigation we may extract the following important conclusions concerning this class of molecules: i) a high density of electronic excited states in the visible/UV energy domain; ii) an important mixing between IL/MLCT and LLCT higher energy states; iii) the presence of low-lying MLCT states, the character of which is very sensitive to the ligands, going from pure $MLCT_{phen}$ to pure $MLCT_{dppz}$ in dppz substituted complexes.

In the RDN analogs the low-lying MLCT states are largely mixed in nature $MLCT_{bpy/phen}$ or $MLCT_{dppz/bpy}$. Interestingly, there is no systematic major contribution of MC and $MLCT_{Phpy}$ excited states to the visible band in the cyclometalated ruthenium complexes. The dppz substituted complexes are characterized by the presence of a shoulder at about 350 nm due to Il_{dppz} transitions. This state could play a key role in electron transfer processes when the complex is intercalated in DNA. Further spectroscopic studies performed on some of the complexes investigated here will aim at determining the DNA/RDC interaction mode and its control on cytotoxic effects.

Acknowledgments

Financial support provided by the ANR program (ANR-09-BLAN-0191-01) and FRC (Strasbourg) is gratefully acknowledged. The quantum chemical calculations have been performed thanks to the computer facilities of the High Performance Computing regional centre of Unistra and on the computer nodes of the LCQS, Strasbourg.

Appendix A. Supplementary data

Supplementary data related to this article can be found at http://dx.doi.org/10.1016/j.jorganchem.2013.08.032.

References

[1] J.-P. Djukic, J.-B. Sortais, L. Barloy, M. Pfeffer, Eur. J. Inorg. Chem. (2009) 817–853.
[2] V. Ritleng, C. Sirlin, M. Pfeffer, Chem. Rev. 102 (2002) 1731–1770;
L. Ackermann, R. Vicente, A.R. Kapdi, Angew. Chem. Int. Ed. 48 (2009) 9792–9826;
P.B. Arockiam, C. Bruneau, P.H. Dixneuf, Chem. Rev. 112 (2012) 5879–5918.
[3] S. Medici, M. Gagliardo, S.B. Williams, P.A. Chase, S. Gladiali, M. Lutz, A.L. Spek, G.P.M. van Klink, G. van Koten, Helv. Chim. Acta 88 (2005) 694–705;
W. Baratta, G. Chelucci, S. Gladiali, K. Siega, M. Toniutti, M. Zanette, E. Zangrando, P. Rigo, Angew. Chem. Int. Ed. 44 (2005) 6214–6219;
J.-B. Sortais, V. Ritleng, A. Voelklin, A. Holuigue, H. Smail, L. Barloy, C. Sirlin, G.K.M. Verzijl, J.A.F. Boogers, A.H.M. de Vries, J.G. de Vries, M. Pfeffer, Org. Lett. 7 (2005) 1247–1250;
N. Pannetier, J.B. Sortais, L. Barloy, J.T. Issenhuth, C. Sirlin, A. Holuigue, P. Lavinia, L. Lefort, J.G. de Vries, M. Pfeffer, Adv. Synth. Catal. 353 (2011) 2844–2852.
[4] S.H. Wadman, J.M. Kroon, K. Bakker, M. Lutz, A.L. Spek, G.P.M. van Klink, G. van Koten, Chem. Commun. (2007) 1907–1909;
T. Bessho, E. Yoneda, J.-H. Yum, M. Guglielmi, I. Tavernelli, H. Iami, U. Rothlisberger, M.K. Nazeeruddin, M.J. Grätzel, J. Am. Chem. Soc. 131 (2009) 5930–5934;
P.G. Bomben, K.C.D. Robson, B.D. Koivisto, C.P. Berlinguette, Coord. Chem. Rev. 256 (2012) 1438–1450.
[5] A.D. Ryabov, Adv. Inorg. Chem. 55 (2004) 201–270;
A.D. Ryabov, V.S. Sukharev, L. Alexandrova, R. Le Lagadec, M. Pfeffer, Inorg. Chem. 40 (2001) 6529;
R. Le Lagadec, L. Rubio, L. Alexandrova, R.A. Toscano, E.V. Ivanova, R. Meskys, V. Laurinavicius, M. Pfeffer, A.D. Ryabov, J. Organomet. Chem. 689 (2004) 4820;
A.D. Ryabov, R. Le Lagadec, H. Estevez, R.A. Toscano, S. Hernandez, L. Alexandrova, V.S. Kurova, A. Fischer, C. Sirlin, M. Pfeffer, Inorg. Chem. 44 (2005) 1626;
R. Le Lagadec, L. Alexandrova, H. Estevez, M. Pfeffer, V. Laurinavicius, J. Razumiene, A.D. Ryabov, Eur. J. Inorg. Chem. (2006) 2735;
A.D. Ryabov, R. Cerón-Camacho, O. Saavedra-Díaz, M.A. Denardo, A. Ghosh, R. Le Lagadec, T.J. Collins, Anal. Chem. 84 (2012) 9096–9100.
[6] (a) C. Gaiddon, P. Jeannequin, P. Bischoff, M. Pfeffer, C. Sirlin, J.-P. Loeffler, J. Pharmacol. Exp. Ther. 315 (2005) 1403;
(b) L. Leyva, C. Sirlin, L. Rubio, C. Franco, R. Le Lagadec, J. Spencer, P. Bischoff, C. Gaiddon, J.-P. Loeffler, M. Pfeffer, Eur. J. Inorg. Chem. 19 (2007) 3055–3066;
(c) X. Meng, M.L. Leyva, M. Jenny, I. Gross, S. Benosman, B. Fricker, S. Harlepp, P. Hebraud, A. Boos, P. Wlosik, P. Bischoff, C. Sirlin, M. Pfeffer, J.-P. Loeffler, C. Gaiddon, Cancer Res. 69 (2009) 5458;
(d) L. Fetzer, B. Boff, M. Ali, M. Xiangjun, J.-P. Collin, C. Sirlin, C. Gaiddon, M. Pfeffer, Dalton Trans. 40 (2011) 8869–8878;
(e) V. Vidimar, X. Meng, M. Mroczek, C. Licona, L. Fetzer, M. Jenny, S. Harlepp, P. Hébraud, C. Sirlin, G. Mellitzer, J.-P. Loeffler, G. Sava, M. Pfeffer, C. Gaiddon, Biochem. Pharmacol. 84 (2012) 1428–1436.
[7] M. Klajner, P. Hebraud, C. Sirlin, C. Gaiddon, S. Harlepp, J. Phys. Chem. 114 (2010) 14041–14047.
[8] A.E. Friedman, J.-C. Chambon, J.-P. Sauvage, N.J. Turro, J.K. Barton, J. Am. Chem. Soc. 112 (1990) 4960–4962.
[9] (a) M. Atsumi, L. González, C. Daniel, J. Photochem. Photobiol. A 190 (2007) 310–320;
(b) C. Gossens, I. Tavernelli, U. Rothlisberger, J. Chem. Theor. Comp. (2007) 1212–1222;
(c) N. Bešker, C. Coletti, A. Marrone, N. Re, J. Phys. Chem. B. 111 (2007) 9955–9964;
L.C. Xu, J. Li, Y. Shen, K.C. Zheng, L.N. Ji, J. Phys. Chem. A. 111 (2007) 273–280;
(d) J. Li, J.C. Chen, L.C. Xu, K.C. Zheng, L.N. Ji, J. Organomet. Chem. 692 (2007) 831–838;
(e) J. Li, L. Xu, J.C. Chen, K.C. Zheng, L.N. Ji, J. Phys. Chem. A. 110 (2006) 8174–8180;
(f) X.W. Liu, J. Li, H. Deng, K.C. Zheng, Z.W. Mao, L.N. Ji, Inorg. Chim. Acta 358 (2005) 3311–3319;
(g) S. Fantacci, F. De Angelis, A. Sgamellotti, A. Marrone, N. Re, J. Am. Chem. Soc. 127 (2005) 14144–14145;
(h) S. Fantacci, F. De Angelis, A. Sgamellotti, N. Re, Chem. Phys. Lett. 396 (2004) 43–48.
[10] D. Ambrosek, P.F. Loos, X. Assfeld, C. Daniel, J. Inorg. Biochem. 104 (2010) 893–901.
[11] I. Ortmans, B. Elias, J.M. Kelly, C. Moucheron, A. Kirsch-De Mesmaeker, Dalton Trans. (2004) 668–676;
J. Olofsson, B. Önfelt, P. Lincoln, J. Phys. Chem. A. 108 (2004) 4391–4398.
[12] C. Metcalfe, H. Adams, I. Haq, J.A. Thomas, Chem. Commun. 10 (2003) 1152–1153.
[13] S. Fernandez, M. Pfeffer, V. Ritleng, C. Sirlin, Organometallics 18 (1999) 2390–2394.
[14] (a) M86-E01078 APEX2 User Manual, Bruker AXS Inc., Madison, USA, 2006;
(b) G.M. Sheldrick, Acta Crystallogr. A46 (1990) 467–473;
(c) G. Sheldrick, SHELXL-97, Universität Göttingen, Göttingen, Germany, 1999;
(d) A.L. Spek, J. Appl, Cryst. 36 (2003) 7–13.
[15] A.D. Becke, J. Chem. Phys. 98 (1993) 5648–5652.
[16] P.J. Stephens, F.J. Devlin, C.F. Chabalowski, M.J. Frisch, J. Phys. Chem. 98 (1994) 11623–11627.
[17] J.P. Perdew, K. Burke, M. Ernzerhof, Phys. Rev. Lett. 77 (1996) 3865–3868.
[18] D. Andrae, U. Häussermann, M. Dolg, H. Stoll, H. Preuss, Theor. Chim. Acta 77 (1990) 123–141.
[19] W.J. Hehre, R. Ditchfield, J.A. Pople, J. Chem. Phys. 56 (1972) 2257–2261.
[20] V. Barone, M. Cossi, J. Phys. Chem. A. 102 (1998) 1995–2001.
[21] J. Bossert, C. Daniel, Coord. Chem. Rev. 252 (2008) 2493–2503;
M. Turki, C. Daniel, S. Zális, A. Vlček Jr., J. van Slageren, D.J. Stufkens, J. Am. Chem. Soc. 123 (2001) 11431–11440;
S. Zális, N. Ben Amor, C. Daniel, Inorg. Chem. 43 (2004) 7978–7985;
N. Ben Amor, S. Zális, C. Daniel, Int. J. Quantum. Chem. 106 (2006) 2458–2469.
[22] E. Runge, E.K.U. Gross, Phys. Rev. Lett. 52 (1984) 997–1000.
[23] M.J. Frisch, G.W. Trucks, H.B. Schlegel, G.E. Scuseria, M.A. Robb, J.R. Cheeseman, J.A. Montgomery Jr., T. Vreven, K.N. Kudin, J.C. Burant, J.M. Millam, S.S. Iyengar, J. Tomasi, V. Barone, B. Mennucci, M. Cossi, G. Scalmani, N. Rega, G.A. Petersson, H. Nakatsuji, M. Hada, M. Ehara, K. Toyota, R. Fukuda, J. Hasegawa, M. Ishida, T. Nakajima, Y. Honda, O. Kitao, H. Nakai, M. Klene, X. Li, J.E. Knox, H.P. Hratchian, J.B. Cross, V. Bakken, C. Adamo, J. Jaramillo, R. Gomperts, R.E. Stratmann, O. Yazyev, A.J. Austin, R. Cammi, C. Pomelli, J.W. Ochterski, P.Y. Ayala, K. Morokuma, G.A. Voth, P. Salvador, J.J. Dannenberg, V.G. Zakrzewski, S. Dapprich, A.D. Daniels, M.C. Strain, O. Farkas, D.K. Malick, A.D. Rabuck, K. Raghavachari, J.B. Foresman, J.V. Ortiz, Q. Cui, A.G. Baboul, S. Clifford, J. Cioslowski, B.B. Stefanov, G. Liu, A. Liashenko, P. Piskorz, I. Komaromi, R.L. Martin, D.J. Fox, T. Keith, M.A. Al-Laham, C.Y. Peng, A. Nanayakkara, M. Challacombe, P.M.W. Gill, B. Johnson, W. Chen, M.W. Wong, C. Gonzalez, J.A. Pople, Gaussian 03, Revision C.02, Gaussian, Inc., Wallingford CT, 2004.
[24] A. Chantzis, T. Very, S. Despax, J.-T. Issenhuth, A. Boeglin, P. Hébraud, M. Pfeffer, A. Monari, X. Assfeld, 2013, submitted for publication.
[25] D.A. Freedmann, J. Evjau, M.K. Panije, K.R. Mann, Inorg. Chem. 40 (2001) 5711.
[26] J.E. Dickeson, L.A. Summers, Aust. J. Chem. 23 (1970) 1023.
[27] C. Gosmini, C. Bassene-Ernst, M. Durandetti, Tetrahedron 65 (2009) 6141–6146.
[28] B. Peña, N.A. Leed, K.R. Dunbar, C. Turro, J. Phys. Chem. C. 116 (2012) 22186–22195.
[29] J.-C. Chambron, J.-P. Sauvage, E. Amouyal, P. Koffi, New J. Chem. 9 (1985) 527;
E. Amouyal, A. Homsi, J.-C. Chambron, J.-P. Sauvage, J. Chem. Soc. Dalton Trans. (1990) 1841–1845.
[30] C. Kuhnt, M. Karnahl, S. Tschierlei, K. Griebenow, M. Schmitt, B. Schäfer, S. Krieck, H. Görls, S. Rau, B. Dietzek, J. Poppac, Phys. Chem. Chem. Phys. 12 (2010) 1357–1368;
M. Karnahl, S. Tschierlei, C. Kuhnt, B. Dietzek, M. Schmitt, J. Popp, M. Schwalbe, S. Krieck, H. Görls, F.W. Heinemann, S. Rau, Dalton Trans. 39 (2010) 2359–2370;
T. Cardinaels, J. Ramaekers, K. Driesen, P. Nockemann, K. Van Hecke, L. Van Meervelt, B. Goderis, K. Binneman, Inorg. Chem. 48 (2009) 2490–2499;
N.J. Lundin, P.J. Walsh, S.L. Howell, A.G. Blackman, K.C. Gordon, Chem. Eur. J. 14 (2008) 11573–11583;
J. Rusanova, S. Decurtins, E. Rusanov, H. Stoeckli-Evans, S. Delahaye, A. Hauser, J. Chem. Soc. Dalton Trans. (2002) 4318–4320;
J.-G. Liu, Q.-L. Zhang, X.-F. Shi, L.-N. Ji, Inorg. Chem. 40 (2001) 5045–5050;
N. Komatsuzaki, R. Katoh, Y. Himeda, H. Sugihara, H. Arakawa, K. Kasuga, J. Chem. Soc. Dalton Trans. (2000) 3053–3054.
[31] M. Buchs, C. Daul, Chimie 52 (1998) 163–166.
[32] R. Blasius, C. Moucheron, A. Kirsch-De-Mesmaker, Eur. J. Inorg. Chem. (2004) 3971–3979.